**Atmospheric
Chemistry
and Physics**

What can ^{14}CO measurements tell us about OH?

M. C. Krol[1,2,3], J. F. Meirink[2], P. Bergamaschi[4], J. E. Mak[5], D. Lowe[6], P. Jöckel[7], S. Houweling[1,2], and T. Röckmann[2]

[1]Netherlands Institute for Space Research (SRON), Utrecht, The Netherlands
[2]Institute for Marine and Atmospheric Research Utrecht (IMAU), Utrecht, The Netherlands
[3]Wageningen University and Research Centre (WUR), Wageningen, The Netherlands
[4]European Commission Joint Research Centre, Institute for Environment and Sustainability, Ispra, Italy
[5]Institute for Terrestrial and Planetary Atmospheres, Stony Brook University, NY, USA
[6]National Institute of Water and Atmospheric Research, Wellington, New Zealand
[7]Max Planck Institute for Chemistry, Mainz, Germany

Abstract. The possible use of ^{14}CO measurements to constrain hydroxyl radical (OH) concentrations in the atmosphere is investigated. ^{14}CO is mainly produced in the upper atmosphere from cosmic radiation. Measurements of ^{14}CO at the surface show lower concentrations compared to the upper atmospheric source region, which is the result of oxidation by OH. In this paper, the sensitivity of ^{14}CO mixing ratio surface measurements to the 3-D OH distribution is assessed with the TM5 model. Simulated ^{14}CO mixing ratios agree within a few molecules ^{14}CO cm^{-3} (STP) with existing measurements at five locations worldwide. The simulated cosmogenic ^{14}CO distribution appears mainly sensitive to the assumed upper atmospheric ^{14}C source function, and to a lesser extend to model resolution. As a next step, the sensitivity of ^{14}CO measurements to OH is calculated with the adjoint TM5 model. The results indicate that ^{14}CO measurements taken in the tropics are sensitive to OH in a spatially confined region that varies strongly over time due to meteorological variability. Given measurements with an accuracy of 0.5 molecules ^{14}CO cm^{-3} STP, a good characterization of the cosmogenic ^{14}CO fraction, and assuming perfect transport modeling, a single ^{14}CO measurement may constrain OH to 0.2–0.3×10^6 molecules OH cm^{-3} on time scales of 6 months and spatial scales of 70×70 degrees (latitude×longitude) between the surface and 500 hPa. The sensitivity of ^{14}CO measurements to high latitude OH is about a factor of five higher. This is in contrast with methyl chloroform (MCF) measurements, which show the highest sensitivity to tropical OH,

mainly due to the temperature dependent rate constant of the MCF–OH reaction. A logical next step will be the analysis of existing ^{14}CO measurements in an inverse modeling framework. This paper presents the required mathematical framework for such an analysis.

1 Introduction

^{14}CO is produced in the atmosphere by thermal neutrons that are induced by cosmic rays. Neutrons are intercepted by nitrogen nuclei forming ^{14}C via ^{14}N(n,p)^{14}C (Libby, 1946). Because of the interaction of the cosmic radiation with the Earth's magnetic field, most of the production takes place at higher latitudes in the upper troposphere and stratosphere. ^{14}C is rapidly oxidized to ^{14}CO with a yield of about 95% (MacKay et al., 1963; Pandow et al., 1960).

Measurements of ^{14}CO have been made at several locations world wide (e.g., Quay et al., 2000; Jöckel et al., 2002; Manning et al., 2005, see also Fig. 2). These measurements indicate that the ^{14}CO mixing ratio at the Earth's surface ranges from less than 5 molecules cm^{-3} (throughout the manuscript the measured and modeled ^{14}CO concentrations are reported at standard temperature and pressure (STP) and are therefore referred to as mixing ratios) in the tropics to more than 25 molecules cm^{-3} STP at high latitudes (Jöckel and Brenninkmeijer, 2002; Röckmann et al., 2002). In the upper troposphere, close to the source region, mixing ratios increase up to 100 molecules cm^{-3} STP (Brenninkmeijer et al., 1995; Jöckel et al., 2002). The low mixing ratios in the troposphere are mainly caused by the action of tropospheric OH that oxidizes ^{14}CO to ^{14}CO$_2$ with a timescale of about

two months. Measurements in the atmosphere may therefore be used to indirectly estimate the abundance of OH (Brenninkmeijer et al., 1992; Jöckel et al., 2002; Mak et al., 1992; Mak and Southon, 1998; Manning et al., 2005; Volz et al., 1981). For instance, the seasonal variation of ^{14}CO at high latitudes clearly signals the oxidizing action of OH in the local summer season. The lower mixing ratios in the tropics are caused by the higher abundance of OH in the tropics, and by the larger distance from the main ^{14}CO production region (Jöckel et al., 2000; Mak and Southon, 1998).

Past efforts to estimate tropospheric OH mostly relied upon atmospheric measurements of methyl chloroform (1,1,1 trichloro-ethane, hereafter MCF), mainly because its source is better constrained (Bousquet et al., 2005; Krol and Lelieveld, 2003; Montzka et al., 2000; Prinn et al., 2005). Due to the phase-out of MCF following the Montreal protocol and its amendments, atmospheric MCF mixing ratios are declining rapidly and have reached current values of only a few parts per trillion. This implies that MCF will lose its usefulness as a species to determine OH concentrations in the near future (Lelieveld et al., 2006). Alternatives are urgently needed and ^{14}CO may be a good candidate in view of its reliable production by natural processes (Brenninkmeijer, 1993).

Several studies attempted to constrain tropospheric OH by ^{14}CO measurements. From a 13-year long record sampled at Baring Head, New Zealand, and Scott Base, Antarctica, Manning et al. (2005) estimated short-term variations of about 10% in high-latitude Southern Hemispheric OH concentrations. Moreover, estimated OH concentrations were anomalously low after the eruption of Mt. Pinatubo in 1991, and after extensive wild fires in Indonesia in 1997.

Earlier, Brenninkmeijer et al. (1992) had derived higher OH concentrations in the SH compared to the NH, based on the fact that the measured ^{14}CO mixing ratios in the NH are higher compared to the SH (see also Quay et al., 2000). ^{14}CO 3-D-transport model studies that account for the different stratosphere-troposphere exchange in both hemispheres, however, do not support such an interhemispheric asymmetry in the OH abundance (Jöckel et al., 2002; Mak et al., 1994).

Mak et al. (1994) compared 2-D model results to ^{14}CO measurements. It was argued that the best estimates of tropospheric OH at that time should be higher than the values used in the model, since ^{14}CO was modeled about 20% too high. Later, the new OH estimates from recalibrated MCF measurements (Prinn et al., 1995) confirmed this finding.

In analyzing ^{14}CO measurements it is important to realize that a measurement is only sensitive to the OH concentration a few months prior to sampling, due to ^{14}CO lifetime, which ranges from weeks in the tropics to months at high latitudes. Moreover, the sampled air mass has encountered a specific OH history along its trajectory from the source region to the sampling site. In contrast to longer-lived species like MCF, this means that a specific ^{14}CO measurement is sensitive to OH within a smaller region of influence. Thus, information

on regional OH can be obtained, given an accurate description of the transport from the production regions to the measurement sites (Volz et al., 1981; Jöckel et al., 2000; Jöckel et al., 2002; Mak and Southon, 1998). Whereas this constraint on regional OH is in principle clear, it has never been quantified.

In this paper a mathematical framework is developed to calculate the sensitivity of single ^{14}CO samples to the OH history. This sensitivity is calculated backward in time using the adjoint of the TM5 model. In contrast to earlier work, the developed framework offers the possibility to investigate the OH sensitivity at high spatial and temporal resolutions and opens the possibility to explore ^{14}CO measurements in a more quantitative manner. The outline of the paper is as follows. The TM5 ^{14}CO version will be described in Sect. 2. The result of forward simulations including a sensitivity analysis is described in Sect. 3. The development of the adjoint TM5 version is discussed in Sect. 4. Section 5 presents the sensitivity of single ^{14}CO (and MCF) measurements to OH as calculated with the adjoint TM5 model. We finish with a discussion and conclusions in Sect. 6.

2 ^{14}CO simulations

2.1 Model description

The TM5 model is a global chemistry transport model (CTM) that has the ability to zoom in over specific geographical regions (Krol et al., 2005). The zoom feature is not used in the current study. TM5 is an off-line model, which means that meteorological fields from a weather forecast model or a climate model are used to drive the model transport. Meteorological fields are taken from the ECMWF (European Centre for Medium Range Weather Forecast) model and coarsened as described in Krol et al. (2005). The TM5 vertical layer structure comprises a sub-set of the 60 layers of the hybrid sigma-pressure system of the ECMWF model. For the current study, we employ a TM5 version without chemistry, except for the oxidation of ^{14}CO by OH. The seasonally varying climatological OH fields constructed by Spivakovsky et al. (2000) are interpolated on a grid of 1° longitude and 1° latitude, and on 60 vertical levels. The high resolution OH field is coarsened to the TM5 resolution, which is taken as 6° longitude×4° latitude and 25 vertical layers. Two-dimensional seasonally varying stratospheric OH fields are taken from the Mainz 2-D stratospheric model (Brühl and Crutzen, 1993). Apart from removal by OH, the small but significant dry deposition of ^{14}CO is taken into account. Deposition velocities are calculated online during model integration based on Ganzeveld et al. (1998).

The upper atmospheric production of ^{14}C by neutrons derived from cosmic rays is strongly modulated by the solar modulation parameter (Φ; Lowe and Allan, 2002). This parameter, which is expressed in MeV, indicates the minimum

amount of energy a cosmic ray particle must have to avoid being deflected by the heliospheric magnetic field during its traverse to Earth.

Different estimates of the height and latitude dependent ^{14}C production distribution are available. In order to compare these and as described in Jöckel et al. (2002), all ^{14}C production distributions were scaled to a (arbitrary) global production of 1 molecule cm^{-2} s^{-1} and subsequently scaled with a common factor that solely depends on the solar modulation parameter (Φ). In the standard case we use the latitudinal and height dependent production distribution calculated by Masarik and Beer (1999), calculated for a heliospheric potential of 650 MeV (intermediate solar cycle conditions). The sensitivity of the simulated ^{14}CO concentrations to the ^{14}C production distribution is investigated by using the alternative distribution function of Lingenfelter (1963). Moreover, to investigate the influence of the selected heliospheric potential on the ^{14}C source distribution function, the distributions were calculated for two alternative heliospheric potentials of 300 and 900 MeV.

The modulation of the global source by the heliospheric potential is calculated according to formula (Eq. 3) in Lowe and Allan (2002), which is based on Masarik and Beer (1999). Monthly values of the heliospheric potentials are presented in Usoskin et al. (2005) and the potentials for 2005 are taken from http://cosmicrays.oulu.fi/phi/ (Usoskin, personal communication, 2006). The ^{14}C source varies considerably during a solar cycle. During a solar maximum, heliospheric shielding potentials maximize and ^{14}C production minimizes. Vice versa, ^{14}C production maximizes during a solar minimum. Figure 1 shows the Heliospheric potential (Usoskin et al., 2005) and the corresponding ^{14}C production efficiency over the 2001–2006 period. The abrupt transition from the solar maximum to the solar minimum in 2004 is clearly visible.

To calculate the ^{14}CO production we assume a ^{14}C to ^{14}CO conversion rate of 0.95 (MacKay et al., 1963; Pandow et al., 1960).

2.2 Forward ^{14}CO simulation results

Model results for the period 2001–2006 will be compared to ^{14}CO measurements, which have been taken at several stations worldwide. From 2004 to 2006, biweekly samples have been collected at American Samoa Observatory (14.3° S, 170.6° W, 77 m), Westmann Islands, Iceland (63.5° N, 20.3° E, 30 m) and at Mauna Loa (19.54° N, 155.6° W, 3400 m). Two other sampling stations that have taken regular measurements are Baring Head, New Zealand (41.4° S, 174.9° E, 85 m), and Scott Base, Antarctica (77.8° S, 166.8° E, 200 m; Manning et al., 2005). Measured ^{14}CO mixing ratios differ from modeled mixing ratios. Modeled ^{14}CO values represent purely cosmogenic ^{14}CO, while measured ^{14}CO contains variable amounts of recycled ^{14}CO due to CO production from natural volatile organic
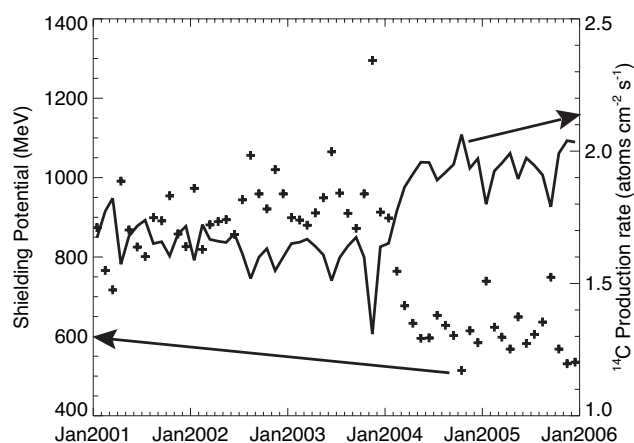

Fig. 1. (crosses, left axis) Monthly values of the shielding potential (Usoskin et al., 2005). (solid line, right axis) ^{14}C production rate calculated from the shielding potential as described in (Lowe and Allan, 2002).

compounds (VOCs) or direct emission from biomass burning (Bergamaschi et al., 2001; Brenninkmeijer, 1993; Mak and Southon, 1998). To account for this recycled fraction in the measurements, we simulated ^{14}C-free CO from direct fossil emissions and from oxidation of fossil CH$_4$. Fossil CH$_4$ was assumed to be 20% (340 ppb) of the atmospheric CH$_4$ burden (Lassey et al., 2007). The modeled fossil CO at the stations was subtracted from the measured CO mixing ratios and the ^{14}C activity of the remaining biogenic CO was taken as 120 percent modern carbon (pmC) (Bergamaschi et al., 2001). This corresponds to roughly 1 molecule ^{14}CO cm^{-3} STP for each 30 ppb of biogenic CO. For baseline conditions the "recycled" ^{14}CO concentrations are typically 1–2 molecules ^{14}CO cm^{-3} STP, with larger values in the Northern Hemisphere.

Figure 2 shows the measurements – with the calculated "recycled" ^{14}CO subtracted – together with cosmogenic ^{14}CO concentrations of the 6-year TM5 simulation (1 January 2000–1 January 2006, hourly concentrations, the first simulation year was discarded as spin-up period). The red lines and symbols represent the available measurements at the stations. For Iceland, Mauna Loa, and Samoa the measurements are still in the validation phase. For this preliminary analysis, outliers were removed by hand and a 3-point moving average was applied to the data. Data points for Baring Head and Scott Base represent samples that were collected during baseline sampling conditions (Manning et al., 2005).

Like the measurements, simulations show minimum ^{14}CO mixing ratios at all stations in local summer, and maxima in local winter. In the tropics (Mauna Loa, Samoa) simulated minima are about 3 molecules ^{14}CO cm^{-3} STP. The simulated values during wintertime are much more variable and range from 5–15 molecules cm^3 STP.
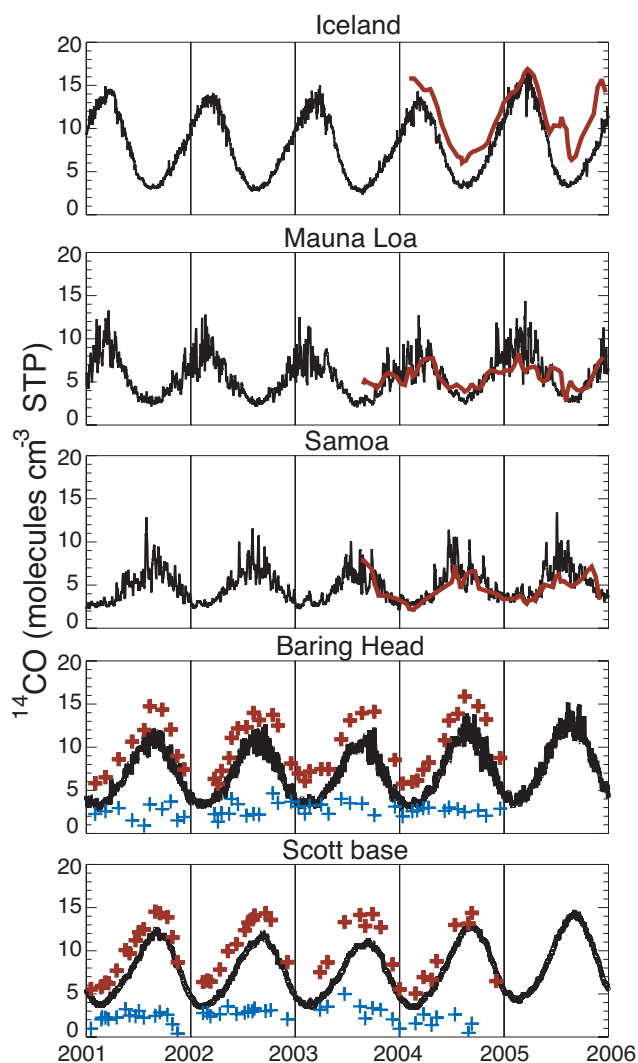
Fig. 2. TM5 simulated hourly cosmogenic ^{14}CO mixing ratios at five measurement stations for Jan-2001 up to Jan-2006. For Iceland, Mauna Loa, and Samoa, a preliminary comparison to measurements that are taken about once every two weeks (red lines, 3-point smoothing applied). For Baring Head and Scott Base a comparison to individual data points is made (red crosses). The blue crosses represent the differences between measurements and model. All measurements were corrected for the recycled ^{14}CO fraction.

High latitude stations show a more regular seasonal variation with generally less short-term variability. The least variable signals are simulated for Iceland and Scott Base, with summertime minima of about 4 molecules cm^{-3} STP and maxima at the end of the winter of about 13–17 molecules cm^{-3} STP.

In local winter, a high latitude reservoir of tropospheric ^{14}CO builds up due to low OH and downward transport from the production region in the stratosphere and upper troposphere (Jöckel et al., 2002; Jöckel et al., 1999; Mak and Southon, 1998). Patches of air from this polar reservoir are
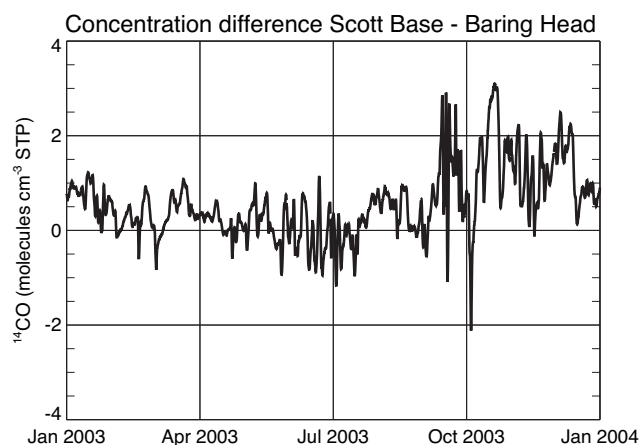

Fig. 3. Simulated mixing ratio difference between Scott Base and Baring Head in 2003.

transported equator-ward. This results in variability in the simulated ^{14}CO mixing ratios at sampling sites at lower latitudes in winter, such as Baring Head, Samoa, and Mauna Loa. Likewise but less frequent, air masses depleted in ^{14}CO originating from the subtropics sometimes reach Iceland in winter. These northward transport events show up as synoptic scale downward excursions of the simulated ^{14}CO mixing ratios. Such events are not simulated for Scott Base.

The comparison between the modeled and corrected ^{14}CO measurements in Fig. 2 shows that the TM5 model is on average predicting too low ^{14}CO mixing ratios at high latitudes. The blue symbols in the lower panels indicate the differences between measurements and model, which appear to be systematic in nature. The model captures the measured seasonal variations very well. The measurements at Samoa and Mauna Loa seem to confirm the enhanced wintertime variability as predicted by the model. The number of samples is too small to verify the model-predicted variability on the short timescales, however.

Manning et al. (2005) report that the mixing ratio difference between Scott Base and Baring Head is generally smaller than 1 molecule cm^{-3} STP, except in October during the seasonal maximum. As shown in Fig. 3, this is in excellent agreement with our simulations. This figure shows that the variability in the Scott Base-Baring Head mixing ratio difference maximizes in September–November. The assumed ^{14}C source height distribution in the upper troposphere and lower stratosphere is a critical factor in modeling the ^{14}CO distribution (Jöckel et al., 2002). This distribution depends on the shielding potential and on the calculation method. The distribution used for the results shown in Fig. 2 was calculated for one fixed shielding potential of 650 MeV. Figure 4 shows model results calculated with the same Masarik and Beer (1999) source distribution, but now obtained for a shielding potential of 300 MeV (note again that all source functions are scaled to a global production of

1 molecule cm^{-2} s^{-1}, see Sect. 2.1). The model results are almost identical, confirming earlier findings (Jöckel et al., 2002). The source distribution of Masarik and Beer (1999) features a relatively large fraction of the ^{14}C production in the stratosphere (62–66%; Jöckel et al., 2002). A significant effect is found when the alternative Lingenfelter (1963) ^{14}C source function is used in the simulations (the effect of the shielding potential is again small). Interestingly, the use of the Lingenfelter source function (with more ^{14}C production in the troposphere) has a more pronounced effect on the high latitudes, bringing the simulations closer to the measurements (see Fig. 4, blue line). The effect on the simulated tropical ^{14}CO concentrations is relatively small. Finally, the employed model resolution plays a small but distinct role. The model resolution influences stratosphere-troposphere exchange, as well as the simulated transport. The first effect is observed at Scott Base, where the high-resolution simulation (3° longitude, 2° latitude, 60 model levels) predicts systematically higher concentrations. This latter effect is clearly observed at Mauna Loa, where the variability in the high-resolution simulation is significantly higher. Thus, the sensitivity simulations show that the model results are sensitive to the ^{14}C source function and the model resolution. Further analysis is beyond the scope of this paper and will be addressed in a future publication.

In general, the TM5 ^{14}CO simulation seems to be realistic and well suited to address the main question of this paper: What is the sensitivity of a ^{14}CO measurement to the OH distribution? Before addressing this question, the adjoint TM5 model will be introduced.

3 The adjoint TM5 model

The development of the adjoint TM5 model was initially motivated by the wish to apply variational data-assimilation methods to the optimization of trace gas emissions (e.g. CO_2, CH_4) using atmospheric measurements (Bergamaschi et al., 2007, Meirink et al., 2008). The applicability of the adjoint TM5 model is, however, not limited to source optimization. For instance, the adjoint of TM5 has been used to determine the sensitivity of atmospheric measurements to (recent) upwind emissions (Gros et al., 2004; Gros et al., 2003). This sensitivity can be expressed by $\frac{\partial \chi(t,x)}{\partial E(t'<t,i,j)}$ for an atmospheric concentration measurement χ at time t and location x and sources $E(i, j)$ that were emitted at times t' before the sampling time t (i and j represent the indices of surface grid boxes in the model). The calculation of these sensitivities requires $n_i \times n_j$ forward simulations in which the sources $E(i, j)$ are perturbed one after the other. The same sensitivity matrix can be calculated with only one adjoint model simulation. To this end, the adjoint model is initiated with a pulse $ad\chi(t, x)$ (with "ad" representing an active adjoint variable, see Appendix A) at the measurement site (location x). After the release of the pulse, the adjoint model is inte-
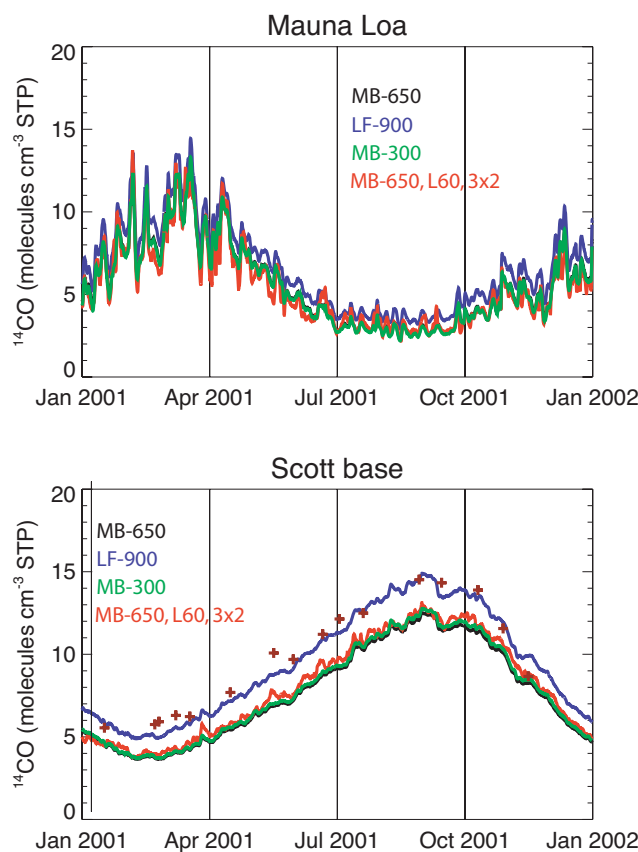

Fig. 4. Results of sensitivity simulations performed for the year 2001 for Mauna Loa and Scott Base. Black: the simulation from Fig. 2 (mostly overlapped by the green line). Blue: the Masarik Beer (1999) ^{14}C source function replaced by the Lingenfelter (1963) source function. Green: ^{14}C source distribution calculated for a shielding potential of 300 MeV instead of 650 MeV. Red: Simulation on a higher model resolution of 3° longitude, 2° latitude and 60 model levels. The dark red crosses represent the measurements.

grated. The pulse $ad\chi(t, x)$ generates an adjoint concentration field that spreads backward in time ($t'<t$) over the model domain. The adjoint concentration field is integrated in time for all surface grid boxes to provide the adjoint emission field $adE(i, j)$. Since transport is described in TM5 by linear operators, the following relation holds:

$$\frac{\partial \chi(t, x)}{\partial E(t'<t, i, j)} = \frac{adE(i, j, t'<t)}{ad\chi(t, x)} \quad (1)$$

The adjoint approach offers large computational advantages, if the sensitivity to emissions (in all model grid boxes) is required for only a limited number of observations (Houweling et al., 1999; Kaminski et al., 1999).

3.1 Adjoint transport

The adjoint code of the two-way nested zoom model TM5 has been constructed largely by manual coding (i.e. no automatic adjoint code generator was used). Details about the adjoint TM5 model are given in Appendix A. For the application described here, the zoom algorithm is not used and only the global model domain is active.

3.2 Adjoint ^{14}CO oxidation

The adjoint TM5 model will be used to calculate the sensitivity of a measurement at a particular station to the 3-D OH distribution $\frac{\partial \chi(t, i', j', k')}{\partial OH(t' < t, i, j, k)}$, stating that a measurement χ in grid box (i', j', k') and time t depends on the 3-D OH at times before the measurement was taken (i, j, k denote the three dimensions of the model array that contains the OH distribution, which varies on a monthly timescale).

As outlined in the previous section, this sensitivity field can be calculated with only one simulation in the adjoint formulation. How should the adjoint model for ^{14}CO oxidation be formulated?

The forward model formulation of the ^{14}CO oxidation by OH in each model grid cell reads (grid box indices i, j, k are dropped):

$$^{14}CO(t+dt) = {}^{14}CO(t) - kOH(t)^{14}CO(t)dt \tag{2a}$$

$$OH(t+dt) = OH(t) \tag{2b}$$

OH denotes the OH concentration (molecules cm^{-3}), which does not change during a particular month in a forward integration, k is the second order rate constant (cm^3 molecules^{-1} s^{-1}) for the reaction between OH and ^{14}CO, and $dt (s)$ is the time step of the model. We are now interested in the sensitivity of ^{14}CO to a perturbation in the OH field. Thus, both OH and ^{14}CO are considered active model variables for which the effect of perturbations (d^{14}CO, dOH) is calculated (see Appendix A). The tangent linear formulation reads:

$$d^{14}CO(t+dt) =$$
$$d^{14}CO(t) - kOH(t)d^{14}CO(t)dt - kdOH(t)^{14}CO(t)dt, \tag{3a}$$

$$dOH(t+dt) = dOH(t). \tag{3b}$$

The matrix formulation of the tangent linear model reads:

$$\begin{bmatrix} d^{14}CO \\ dOH \end{bmatrix}^{(t+dt)} =$$
$$\begin{bmatrix} 1-kOH(t)dt & -k^{14}CO(t)dt \\ 0 & 1 \end{bmatrix} \begin{bmatrix} d^{14}CO \\ dOH \end{bmatrix}^{(t)}. \tag{4}$$

The adjoint code is derived by transposing the forward matrix (Giering and Kaminski, 1998):

$$\begin{bmatrix} ad^{14}CO \\ adOH \end{bmatrix}^{(t)} =$$
$$\begin{bmatrix} 1-kOH(t)dt & 0 \\ -k^{14}CO(t)dt & 1 \end{bmatrix} \begin{bmatrix} ad^{14}CO \\ adOH \end{bmatrix}^{(t+dt)}, \tag{5}$$

where ad^{14}CO and $adOH$ are adjoint model variables. The adjoint code then reads:

$$ad^{14}CO(t) = ad^{14}CO(t+dt) - kOH(t)ad^{14}CO(t+dt)dt \tag{6a}$$

$$adOH(t) = adOH(t+dt) - k^{14}CO(t)ad^{14}CO(t+dt)dt \tag{6b}$$

The ad^{14}CO variable tracks the adjoint ^{14}CO field that is generated by a pulse released at a measurement station. This pulse is transported backward in time in the adjoint model and is chemically destroyed by OH, similar to ^{14}CO in the forward model. The $adOH$ field accumulates the product of the forward ^{14}CO field (kg m^{-3}) and the adjoint ^{14}CO field (kg^{-1} m^3), multiplied by kdt (molecules^{-1} cm^3). The units of $adOH$ are therefore (molecules^{-1} cm^3). The $adOH$ field can be integrated over arbitrary time intervals and spatial domains. In practical applications the monthly integrated $adOH$ values can be used to optimize monthly OH fields.

Note that the forward ^{14}CO field has to be available during the adjoint integration. To accomplish this, the forward ^{14}CO fields are stored during the forward model integration. The sensitivity of a ^{14}CO measurement to OH now follows, equivalent to Eq. (1), from:

$$\frac{\partial \chi(t)}{\partial OH(i, j, k)} = \frac{adOH(i, j, k)}{ad\chi(t)}, \tag{7}$$

which states that the adjoint OH field calculated for a unit pulse $ad\chi(t)$ at the measurement location represents the sensitivity of a measurement at that location and time to the 3-D OH field.

The correct implementation of the adjoint version of TM5, including the ^{14}CO oxidation scheme, was verified by applying the adjoint test as outlined in the Appendix.

3.3 Adjoint OH simulations

Adjoint simulations are initialized by the simultaneous release of ^{14}CO pulses at five measurement stations where regular measurements are taken (Iceland, Mauna Loa, Samoa, Baring Head, and Scott Base). The size of the pulses is not critical in the linear approach and we use equal pulses of 2.5 molecules ^{14}CO cm^{-3} STP at all five stations, which are added during a three-hour period.

Figure 5 shows the vertically integrated $adOH$ field, expressed per kg air. For visualization, scaling with grid-box air masses is applied to the calculated 3-D $adOH$ field. The necessity of this air mass scaling can best be understood from Eq. (7). In the equivalent forward sensitivity calculation, the
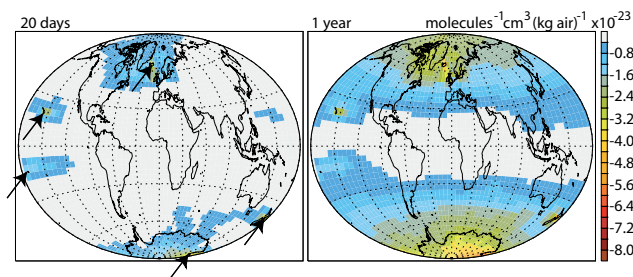
Fig. 5. Mass-weighed vertically integrated adOH-field, calculated by the release of five pulses of 2.5 molecules ^{14}CO cm^{-3} STP at the five measurement stations (Iceland, Mauna Loa, Samoa, Baring Head, Scott Base). Pulses were released on 1 January 2006. Left: the adOH field after 20 days of integration. Right: after one year of integration. The black arrows in the leftmost panel indicate the locations where the ^{14}CO pulses were released.

3-D OH field would be perturbed grid-box by grid-box. In a forward calculation of $\frac{\partial \chi(t)}{\partial OH(i,j,k)}$ one would normally add a small fixed amount dOH (e.g. 10^4 molecules cm^{-3}) to the OH concentration in each grid-box and calculate the impact $d\chi$ of this perturbation at the measurement stations. Since the grid-boxes in the model are not of equal size, this procedure implies larger perturbations (counted in molecules OH) in large grid boxes, simply because the amount of OH added scales with the air mass that is present in each grid box. The variation in the air masses over the grid boxes should be taken into account when the adjoint OH field is visualized. The unit of the visualized adjoint OH field is therefore (cm^3 molecules^{-1}(kg air)$^{-1}$). The sign of the sensitivity is negative since lower OH leads to higher ^{14}CO. A larger absolute value of the adjoint OH field implies that less OH is needed to cause a signal at the measurement sites (i.e. that the sensitivity to OH is larger). The field is shown after 20 days of integration (left panel Fig. 5) and after one year of integration (right panel). After about one year – about 6 times the atmospheric lifetime of ^{14}CO – the adjoint OH integration is almost completely converged. Note that the yellow/red colors correspond to high sensitivity. Equations 6a and b contain the factors that control the magnitude of the adOH field. These factors are:

1. The ad^{14}CO field generated by the pulses released at the measurement stations (Eq. 6b). This field is subject to removal by the reaction with OH (Eq. 6a)

2. The ^{14}CO field from the forward model integrations (Eq. 6b)

3. The reaction rate k (Eq. 6b)

Apart from these factors, transport also plays an important role. Zonal transport is faster at the poles due to the smaller circumpolar distances. Due to higher OH in the tropics and the great distance of the tropics from the source region, the
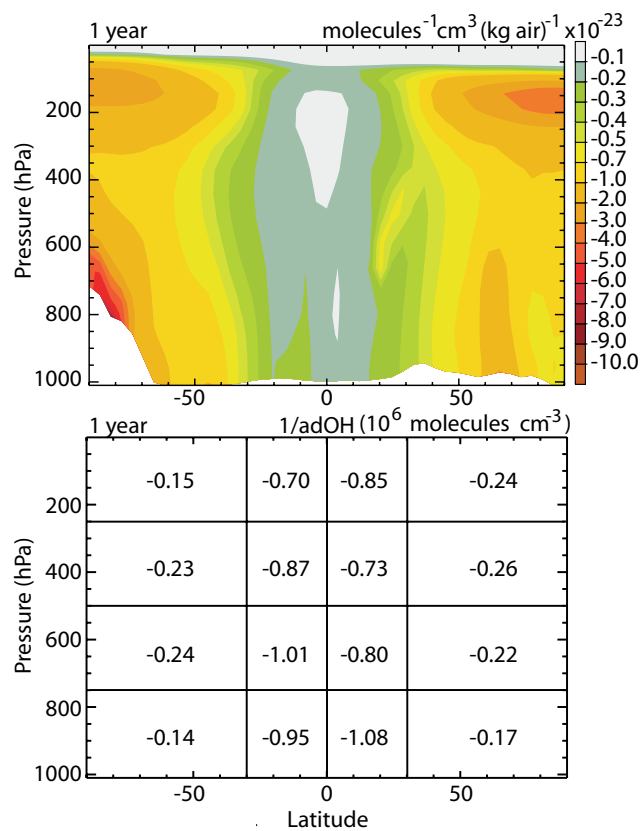

Fig. 6. Upper panel: Mass-weighted zonal integral of the adOH field after one year of integration (see legend Fig. 5). Note the nonlinear color scale. Lower panel: The inverse of the adOH field after one year, integrated over boxes of about equal mass in units 10^6 molecules cm^{-3}.

tropical ^{14}CO field from the forward model integration shows smaller concentrations than at high latitudes.

The longer integration has mainly an impact on the adOH field at higher latitudes. But even at high latitudes the signal of the first 20 days around the measurement stations remains visible. The higher sensitivity towards the poles is explained by the longer lifetime of the adjoint ^{14}CO field (lower OH) in combination with a higher value of the ^{14}CO field from the forward simulation.

The ^{14}CO field from the forward simulation maximizes in the source regions around the high-latitude tropopause. Although the ad^{14}CO field generated by the pulses is rather quickly oxidized in the lower atmosphere (Eq. 6a), a part of the ad^{14}CO tracer propagates upward and will reach the ^{14}CO source region. This is especially true for the high latitude winter season when the ^{14}CO lifetime is long. Due to the pressure-dependent rate constant between OH and ^{14}CO, the lifetime of ^{14}CO is rather long in the upper troposphere (Jöckel et al., 2000). The lingering ad^{14}CO field, combined with the high values of the forward ^{14}CO field, integrates (Eq. 6b) to high values of adOH, as shown in Fig. 6 (note
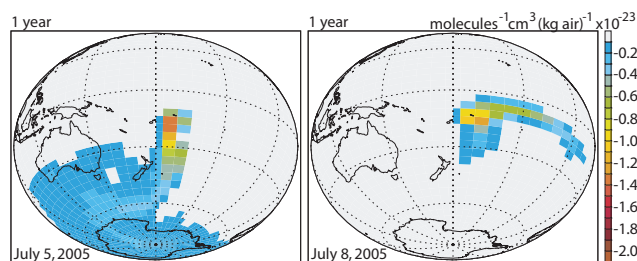
Fig. 7. Mass-weighted vertically integrated adOH field for a single pulse (2.5 molecules ^{14}CO cm^{-3} STP) released at Samoa. Left: pulse released at 5 July 2005, 00:00 GMT. Right: pulse released at 8 July 2005, 00:00 GMT. The mixing ratios in the forward simulation amount to 13.3 and 6.9 molecules ^{14}CO cm^{-3} STP, respectively.

the non-linear color scale). In the tropics the sensitivity is generally much lower.

The lower panel of Fig. 6 integrates the adOH field (integrated over one year) over atmospheric boxes of about equal mass. Due to these equal masses, the scaling is not longer necessary and the numbers represent $(ad\text{OH})^{-1}$ in the unit 10^6 molecules cm^{-3}. Note that these numbers have been obtained by spatial integration of adOH and subsequent inversion of the result. These numbers can be interpreted as the OH perturbations needed to cause the 2.5 molecules ^{14}CO cm^{-3} STP pulses at the measurement stations (see Eq. 7). Thus, the network of five stations is 4–6 times more sensitive to OH perturbations at high latitudes than to similar perturbations in the tropics.

The sensitivity of a ^{14}CO measurement depends on the season in which a sample is taken (not shown). During the high latitude winter season, released pulses survive oxidation for longer periods, which implies that the adjoint ^{14}CO field contributes longer to the adOH integration.

To analyze the sensitivity of tropical ^{14}CO measurements for regional OH in the tropics, we will focus on the Samoa measurement location (14.3° S). First, it is observed that the fate of the pulses just after release depends strongly on the meteorological situation. As an example, a period is selected (4–8 July 2005) in which the simulated ^{14}CO mixing ratio varies strongly at Samoa. Simulated mixing ratios at Samoa change from 13.3 molecules ^{14}CO cm^{-3} STP at 5 July (00:00 GMT) to 6.9 molecules ^{14}CO cm^{-3} STP at 8 July (00:00 GMT; see Fig. 2). Figure 7 shows the calculated adjoint OH fields from two separate pulses released at Samoa at those times. The 8 July pulse is mainly sensitive to tropical OH. This could be expected from the low ^{14}CO mixing ratio that signals an air mass that has been for quite a while in the tropics. In contrast, the 5 July pulse is also sensitive to high latitude OH. The high ^{14}CO mixing ratio in the forward simulation is clearly caused by transport from the ^{14}CO pool that is present at high latitudes in winter. Apparently, the sensitivity of a single ^{14}CO measurement to OH depends strongly on the air mass from which the sample is taken. Thus, Fig. 7
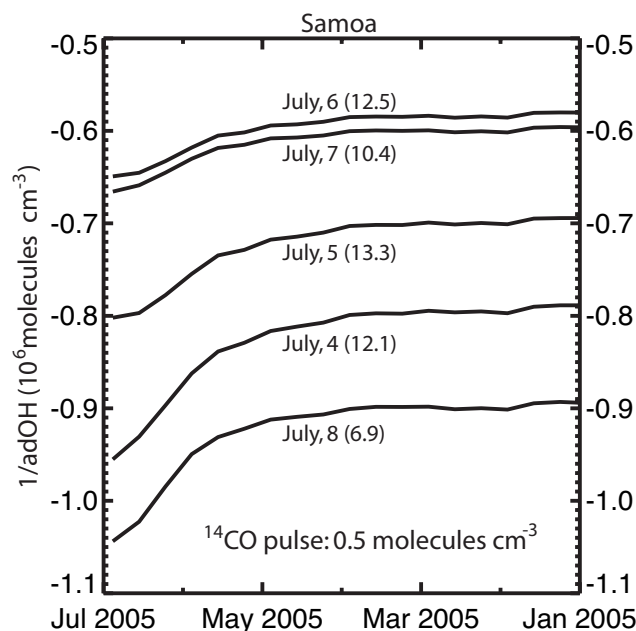

Fig. 8. Convergence of $(ad\text{OH})^{-1}$ integrated over an atmospheric box around Samoa (180° E–162° E, 38° S–6° S, surface-500 hPa) for pulses of 0.5 molecules ^{14}CO cm^{-3} STP released at five consecutive days at Samoa. The values in parentheses correspond to the simulated mixing ratios at Samoa (molecules cm^{-3} STP).

illustrates that in a tropical air mass a measurement is sensitive to regional OH close to the measurement location. In an air mass that originates from high latitudes, the measurement has additional sensitivity to OH at these higher latitudes. To highlight the sensitivity of ^{14}CO measurements to the regional OH concentration and the variability in this sensitivity, a ^{14}CO pulse of 0.5 molecules cm^{-3} STP was released during a three hour time period at five consecutive days. The pulse size is now chosen to represent the ^{14}CO measurement accuracy. Figure 8 shows the convergence of $(ad\text{OH})^{-1}$ for these five ^{14}CO pulses. The adOH field is integrated over a relatively small tropospheric box (see legend) and $(ad\text{OH})^{-1}$ can thus be interpreted as the OH perturbation (in molecules cm^{-3}) in the box that causes a detectable perturbation at the Samoa station. Note that the convergence of the adOH in this lower tropospheric box is rather fast. The average sensitivity of the Samoa measurement to regional OH is calculated as $-0.71\pm0.13\times10^6$ molecules cm^{-3} for a pulse of 0.5 molecules ^{14}CO cm^{-3} STP during this period. This corresponds to about 50% of the estimated OH concentration in this box (Spivakovsky et al., 2000).

The dependence on the size of the integration area around Samoa is explored in Fig. 9. Obviously, a larger area of OH perturbation results in a larger effect on the Samoa measurement. Consequently, $(ad\text{OH})^{-1}$ is more negative for a larger integration area. The five lines in Fig. 9 are obtained by integrating the largest surface – 500 hPa adOH columns around
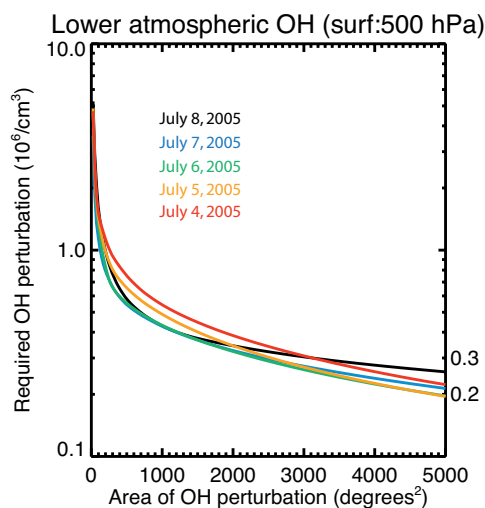
Fig. 9. Value of $(ad\mathrm{OH})^{-1}$ as a function of the area around Samoa (expressed in degrees^2 and integrated from the surface to 500 hPa) for pulses of -0.5 molecules ^{14}CO cm^{-3} STP released at five consecutive days at Samoa. Note that the adOH is integrated over the grid boxes with the largest sensitivity.
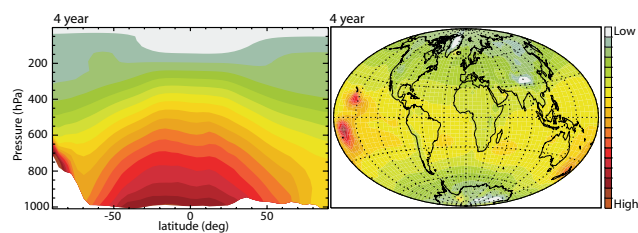

Fig. 10. The adOH field calculated for methyl chloroform (MCF) pulses released at the five measurement stations after 4 years of integration. The required field from the forward simulation (Eq. 6b) is assumed to be well mixed. Left: Mass-weighted zonal integral (compare to Fig. 6). Right: Mass-weighted vertical integral (compare to Fig. 5). Only the distribution is considered important here. Red colors indicate a high sensitivity to OH (a strongly negative adOH field) and green colors a low sensitivity.

Samoa. From Fig. 9 it follows that a measurements at Samoa is predicted to change by -0.5 molecules ^{14}CO cm^{-3} STP if OH around the Samoa station is perturbed by about 0.2–0.3×10^6 molecules OH cm^{-3} in a region with a size of 5000 degrees^2 (about 70×70 degrees) from the surface to the 500 hPa level. Note that this sensitivity corresponds to only one ^{14}CO measurement and an OH perturbation that lasts for 6 months (January–July 2005). This value implies that ^{14}CO measurements in the tropics can constrain regional OH to about 15–25%, given accurate measurements, and assuming perfect transport modeling. Moreover, the regional sensitivity implies that at least five (360°/70°) tropical ^{14}CO sampling sites are required to be sensitive to OH at all longitudes in the tropics.

Finally, we want to compare the OH sensitivity of ^{14}CO measurements to the sensitivity of MCF measurements. Thus, we released MCF pulses (an arbitrary amount, since we are primarily interested in the distribution of the adOH field) instead of ^{14}CO pulses at the five measurement stations. Since the lifetime of MCF is much longer than that of ^{14}CO (5 years compared to two months), we assumed a well-mixed forward MCF field (at an arbitrary fixed concentration) in the integration of the adOH field. In practice, ^{14}CO(t) was replaced by a constant in Eq. (6b). Moreover, the pressure dependent rate constant of the OH+^{14}CO reaction was replaced by the temperature dependent rate constant of the OH+MCF reaction. Figure 10 depicts the resulting adOH field after four years of integration. Note again that we focus here on the distribution of the sensitivity rather than on the absolute values. Compared to ^{14}CO, the vertically integrated adOH field from MCF (right panel) shows a much

higher sensitivity in the tropics. Moreover, the sensitivity is more spread out, although the higher sensitivity close to the release points can still be discerned after four years of integration. Also, the orography influences the adOH field. The zonally integrated adOH field shows that the sensitivity of MCF to OH is mainly controlled by the temperature dependent rate constant, although the Scott Base release point remains clearly visible in the zonal average. An important factor here is the long lifetime of MCF compared to the atmospheric mixing time, which causes a rather well mixed adMCF field some months after the release of the pulses. As a result, the backward integration of the adOH field depends only on the spatial distribution of the rate constant k (Eq. 6b).

4 Conclusions

The main focus of this paper is on the sensitivity of single ^{14}CO measurements to the 3-D OH field. Calculations with the adjoint TM5 model lead to the following conclusions:

- ^{14}CO mixing ratios, especially in the tropics, are sensitive to OH relatively close to the measurement station

- Sensitivity to OH at hemispheric scales is strongly influenced by the origin of the air mass that is transported to the measurement location

- ^{14}CO mixing ratio measurements of the current measurement network are about 5 times more sensitive to high latitude OH than to tropical OH and show sensitivity to upper atmospheric OH at high latitudes

- A single measurement at a tropical measurement site like Samoa is sensitive to regional OH variations of 0.2–0.3×10^6 molecules cm^{-3} in a 6-month time period

Whether or not it will be possible to use ^{14}CO measurements to constrain OH will depend on the amount of measurements available and on our ability to accurately model the ^{14}CO transport. Critical issues are not only the transport of ^{14}CO from the source regions to the lower troposphere (like stratosphere-stratosphere exchange), but also the transport during the last few days prior to the sampling. Modern tracer transport models show increased capabilities to simulate these processes accurately and consequently offer new possibilities to explore ^{14}CO measurements.

The sensitivity of ^{14}CO measurements to OH contrasts strongly with the sensitivity of MCF measurements. A comparison of Figs. 6 and 10 shows that an MCF mixing ratio measurement is relatively much more sensitive to tropical OH. The adjoint formulation of the problem offers an explanation. The factors that control the differences are the rate constant (pressure dependent for ^{14}CO+OH, temperature dependent for MCF+OH), and the lifetime (much shorter for ^{14}CO). Moreover, the high sensitivity of the ^{14}CO mixing ratio to high latitude upper atmospheric OH is caused by the high ^{14}CO mixing ratios in the source region.

A logical next step following this study will be the exploration of the available ^{14}CO measurements in a data-assimilation approach. In such a framework, both the sources and the sinks of ^{14}CO are optimized by minimizing the differences between measurements and model predictions. This will give a more definite answer to the question how the ^{14}CO measurements constrain OH. Based on the current study it can be concluded that constraints on tropical OH will have a regional character.

Appendix A

The adjoint TM5 model

The adjoint transport model TM5 accounts for the fact that TM5 allows two-way nested zooming. However, the current study does not use the zoom capability.

As described in more detail in (Krol et al., 2005), TM5 uses operator splitting with separate subroutines for x, y, z-advection, chemistry, emission, and vertical transport (convection and diffusion). This modular structure of the forward model is used to construct subroutines that are the adjoint of the forward routines. In this way, the correct coding of the various routines could be checked by dedicated testing routines.

Variables in the adjoint model are either active or inactive (Giering and Kaminski, 1998). Active variables represent those variables that are used in the calculation of the tangent linear derivatives (e.g. the adjoint concentration field (ad^{14}CO) and the adjoint emissions (adE) from Sect. 3). Inactive variables must be identical in the forward and adjoint integrations. Examples are temperature, humidity, and winds. In an offline model like TM5 these inactive variables

are stored in files and the adjoint model simply reads the same files as the forward model.

The adjoint code follows directly when the forward model is written in the form of matrices (Giering and Kaminski, 1998). The adjoint code follows by simply taking the transpose of these matrices. This procedure has been followed for the TM5 model.

A rigorous and general way to check the correct coding of the adjoint model uses a general property of a linear model:

$$< Lx, y >=< x, L^T y > \qquad (A1)$$

Here L denotes the tangent linear forward model and L^T the adjoint of the tangent linear model. Since the TM5 transport model (in the absence of any chemistry) is a linear model, it represents already the tangent linear model. x denotes the model state (all active variables) and y is the adjoint model state, and $<>$ denotes an inner product. A correct coding of the adjoint implies that the equality of Eq. (A1) holds for any state x and y. Note that Eq. 1 from the main text is just a specific case of Eq. A1 with x being zero apart from $\partial E(t' < t, i, j)$ and y being zero except from $ad\chi(t,x)$. The adjoint TM5 was tested with a random choice of the forward (x) and adjoint (y) states. The equality of Eq. (A1) was verified to be correct up to O(10^{-14}) for integration times of up to 1 year.

Edited by: A. Volz-Thomas

References

Bergamaschi, P., Frankenberg, C., Meirink, J. F., Krol, M., Dentener, F., Wagner, T., Platt, U., Kaplan, J. O., Körner, S., Heimann, M., Dlugokencky, E. J., and Goede, A.: Satellite chartography of atmospheric methane from SCIA-MACHY onboard ENVISAT – 2: Evaluation based on inverse model simulations, J. Geophys. Res.-Atmos., 112, D02304 , doi:10.1029/2006JD007268, 2007.

Bergamaschi, P., Lowe, D. C., Manning, M. R., Moss, R., Bromley, T., and Clarkson, T. S.: Transects of atmospheric CO, CH$_4$, and their isotopic composition across the Pacific: Shipboard measurements and validation of inverse models, J. Geophys. Res.-Atmos., 106, 7993–8011, 2001.

Bousquet, P., Hauglustaine, D. A., Peylin, P., Carouge, C., and Ciais, P.: Two decades of OH variability as inferred by an inversion of atmospheric transport and chemistry of methyl chloroform, Atmos. Chem. Phys., 5, 2635–2656, 2005, http://www.atmos-chem-phys.net/5/2635/2005/.

Brenninkmeijer, C. A. M.: Measurement of the Abundance of (CO)-C-14 in the Atmosphere and the C-13 C-12 and O-18 O-16 Ratio of Atmospheric CO with Applications in New-Zealand and Antarctica, J. Geophys. Res.-Atmos., 98, 10 595–10 614, 1993.

Brenninkmeijer, C. A. M., Lowe, D. C., Manning, M. R., Sparks, R. J., and van Velthoven, P. F. J.: The C-13, C-14 and O-18 isotopic composition of CO, CH$_4$, and CO$_2$ in the higher southern latitudes lower stratosphere, J. Geophys. Res.-Atmos., 100, 26 163–26 172, 1995.

Brenninkmeijer, C. A. M., Manning, M. R., Lowe, D. C., Wallace, G., Sparks, R. J., and Volz Thomas, A.: Interhemispheric Asymmetry in OH Abundance Inferred from Measurements of Atmospheric (CO)-C-14, Nature, 356, 50–52, 1992.

Brühl, C. and Crutzen, P. J.: The MPIC 2-D model, NASA Ref. Publ., 1292, 103–104, 1993.

Ganzeveld, L., Lelieveld, J., and Roelofs, G. J.: A dry deposition parameterization for sulfur oxides in a chemistry and general circulation model, J. Geophys. Res.-Atmos., 103, 5679–5694, 1998.

Giering, R. and Kaminski, T.: Recipes for adjoint code construction, Acm Transactions on Mathematical Software, 24, 437–474, 1998.

Gros, V., Williams, J., Lawrence, M. G., von Kuhlmann, R., van Aardenne, J., Atlas, E., Chuck, A., Edwards, D. P., Stroud, V., and Krol, M.: Tracing the origin and ages of interlaced atmospheric pollution events over the tropical Atlantic Ocean with in situ measurements, satellites, trajectories, emission inventories, and global models, J. Geophys. Res.-Atmos., 109, D22306, doi:10.129/2004JD004846, 2004.

Gros, V., Williams, J., van Aardenne, J. A., Salisbury, G., Hofmann, R., Lawrence, M. G., von Kuhlmann, R., Lelieveld, J., Krol, M., Berresheim, H., Lobert, J. M., and Atlas, E.: Origin of anthropogenic hydrocarbons and halocarbons measured in the summertime European outflow (on Crete in 2001), Atmos. Chem. Phys., 3, 1223–1235, 2003,
http://www.atmos-chem-phys.net/3/1223/2003/.

Houweling, S., Kaminski, T., Dentener, F., Lelieveld, J., and Heimann, M.: Inverse modeling of methane sources and sinks using the adjoint of a global transport model, J. Geophys. Res., 104, 26 137–26 160, 1999.

Jöckel, P. and Brenninkmeijer, C. A. M.: The seasonal cycle of cosmogenic (CO)-C-14 at the surface level: A solar cycle adjusted, zonal-average climatology based on observations, J. Geophys. Res.-Atmos., 107, 4656, doi:10.1029/2001JD001104, 2002.

Jöckel, P., Brenninkmeijer, C. A. M., and Lawrence, M. G.: Atmospheric response time of cosmogenic (CO)-C-14 to changes in solar activity, J. Geophys. Res.-Atmos., 105, 6737–6744, 2000.

Jöckel, P., Brenninkmeijer, C. A. M., Lawrence, M. G., Jeuken, A. B. M., and van Velthoven, P. F. J.: Evaluation of stratosphere-troposphere exchange and the hydroxyl radical distribution in three-dimensional global atmospheric models using observations of cosmogenic (CO)-C-14, J. Geophys. Res.-Atmos., 107, 4446, doi:10.1029/2001JD001324, 2002.

Jöckel, P., Lawrence, M. G., and Brenninkmeijer, C. A. M.: Simulations of cosmogenic (CO)-C-14 using the three-dimensional atmospheric model MATCH: Effects of C-14 production distribution and the solar cycle, J. Geophys. Res.-Atmos., 104, 11 733–11 743, 1999.

Kaminski, T., Heimann, M., and Giering, T.: A coarse grid three dimensional global inverse model of the atmospheric transport, 1, Adjoint Model and Jacobian Matrix, J. Geophys. Res., 104, 18 535–18 553, 1999.

Krol, M., Houweling, S., Bregman, B., van den Broek, M., Segers, A., van Velthoven, P., Peters, W., Dentener, F., and Bergamaschi, P.: The two-way nested global chemistry-transport zoom model TM5: algorithm and applications, Atmos. Chem. Phys., 5, 417–432, 2005,
http://www.atmos-chem-phys.net/5/417/2005/.

Krol, M. and Lelieveld, J.: Can the variability in tropospheric OH be deduced from measurements of 1,1,1-trichloroethane (methyl chloroform)?, J. Geophys. Res., 108, 4125, doi:10.1029/2002JD002423, 2003.

Lassey, K. R., Lowe, D. C., and Smith, A. M.: The atmospheric cycling of radiomethane and the "fossil fraction" of the methane source, Atmos. Chem. Phys., 7, 2141–2149, 2007,
http://www.atmos-chem-phys.net/7/2141/2007/.

Lelieveld, J., Brenninkmeijer, C. A. M., Joeckel, P., Isaksen, I. S. A., Krol, M. C., Mak, J. E., Dlugokencky, E., Montzka, S. A., Novelli, P. C., Peters, W., and Tans, P. P.: New Directions: watching over tropospheric hydroxyl (OH), Atmos. Environ., 40, 5741–5743, 2006.

Libby, W. F.: Atmospheric helium and radiocarbon from cosmic radiation, Phys. Rev., 69, 671–672, 1946.

Lingenfelter, R. E.: Production of carbon 14 by cosmic-ray neutrons, Rev. Geophys., 1, 35–55, 1963.

Lowe, D. C. and Allan, W.: A simple procedure for evaluating global cosmogenic C-14 production in the atmosphere using neutron monitor data, Radiocarbon, 44, 149–157, 2002.

MacKay, C., Pandow, M., and Wolfgang, R.: On the chemistry of natural radiocarbon, J. Geophys. Res., 68, 3929–3931, 1963.

Mak, J. E., Brenninkmeijer, C. A. M., and Manning, M. R.: Evidence for a Missing Carbon-Monoxide Sink Based on Tropospheric Measurements of (CO)-C-14, Geophys. Res. Lett., 19, 1467–1470, 1992.

Mak, J. E., Brenninkmeijer, C. A. M., and Tamaresis, J.: Atmospheric (CO)-C-14 Observations and Their Use for Estimating Carbon-Monoxide Removal Rates, J. Geophys. Res.-Atmos., 99, 22 915–22 922, 1994.

Mak, J. E., and Southon, J. R.: Assessment of tropical OH seasonality using atmospheric (CO)-C-14 measurements from Barbados, Geophys. Res. Lett., 25, 2801–2804, 1998.

Manning, M. R., Lowe, D. C., Moss, R. C., Bodeker, G. E., and Allan, W.: Short-term variations in the oxidizing power of the atmosphere, Nature, 436, 1001–1004, 2005.

Masarik, J. and Beer, J.: Simulation of particle fluxes and cosmogenic nuclide production in the Earth's atmosphere, J. Geophys. Res.-Atmos., 104, 12 099–12 111, 1999.

Meirink, J. F., Bergamaschi, P., and Krol, M. C.: Technical Note: Four-dimensional variational data assimilation for inverse modelling of atmospheric methane emissions: method and comparison with synthesis inversion, Atmos. Chem. Phys. Discuss., 8, 12 023–12 052, 2008,
http://www.atmos-chem-phys-discuss.net/8/12023/2008/.

Montzka, S. A., Spivakovsky, C. M., Butler, J. H., Elkins, J. W., Lock, L. T., and Mondeel, D. J.: New observational constraints for atmospheric hydroxyl on global and hemispheric scales, Science, 288, 500–503, 2000.

O'Brien, K., de la Zerda Lerner, A., Shea, M. A., and Smart, D. F.: The production of cosmogenic isotopes in the Earth's atmosphere and their inventories, in: The Sun in Time, edited by: Sonett, C. P., Giampapa, M. S., and Matthews, M. S., et al., Univ. of Arizona Press, Tucson, AZ, USA, 317–342, 1991.

Pandow, M., MacKay, C., and Wolfgang, R.: The reaction of atomic carbon with oxygen: Significance for the natural carbon cycle, J. Inorg. Nucl. Chem., 14, 153–158, 1960.

Prinn, R. G., Huang, J., Weiss, R. F., Cunnold, D. M., Fraser, P. J., Simmonds, P. G., McCulloch, A., Harth, C., Reimann, S.,

Salameh, P., O'Doherty, S., Wang, R. H. J., Porter, L. W., Miller, B. R., and Krummel, P. B.: Evidence for variability of atmospheric hydroxyl radicals over the past quarter century, Geophys. Res. Lett., 32, L07809, doi:10.1029/2004GL022228, 2005.

Prinn, R. G., Weiss, R. F., Miller, B. R., Huang, J., Alyea, F. N., Cunnold, D. M., Fraser, P. J., Hartley, D. E., and Simmonds, P. G.: Atmospheric Trends and Lifetime of CH_3CCl3 and Global OH Concentrations, Science, 269, 187–192, 1995.

Quay, P., King, S., White, D., Brockington, M., Plotkin, B., Gammon, R., Gerst, S., and Stutsman, J.: Atmospheric (CO)-C-14: A tracer of OH concentration and mixing rates, J. Geophys. Res.-Atmos., 105, 15 147–15 166, 2000.

Röckmann, T., Jöckel, P., Gros, V., Braunlich, M., Possnert, G., and Brenninkmeijer, C. A. M.: Using C-14, C-13, O-18 and O-17 isotopic variations to provide insights into the high northern latitude surface CO inventory, Atmos. Chem. Phys., 2, 147–159, 2002,
http://www.atmos-chem-phys.net/2/147/2002/.

Spivakovsky, C. M., Logan, J. A., Montzka, S. A., Balkanski, Y. J., Foreman-Fowler, M., Jones, D. B. A., Horowitz, L. W., Fusco, A. C., Brenninkmeijer, C. A. M., Prather, M. J., Wofsy, S. C., and McElroy, M. B.: Three-dimensional climatological distribution of tropospheric OH: Update and evaluation, J. Geophys. Res.-Atmos., 105, 8931–8980, 2000.

Usoskin, I. G., Alanko-Huotari, K., Kovaltsov, G. A., and Mursula, K.: Heliospheric modulation of cosmic rays: Monthly reconstruction for 1951–2004, J. Geophys. Res.-Space Phys., 110, A12108, doi:10.1029/2005JA011250, 2005.

Volz, A., Ehhalt, D. H., and Derwent, R. G.: Seasonal and latitudinal variation of [14]CO and the tropospheric concentration of OH radicals, J. Geophys. Res., 86, 5163–5171, 1981.